1 D Aftertreatment Simulation and Model Calibration for Euro VII Engines

Master thesis in the Department of Chemistry and Chemical Engineering, on behalf of the Department of Industrial and Materials Science

Chalmers University of Technology

Dennis Wang (lihaow@chalmers.se, dennis.wang@scania.com)

June 26th, 2026

Supervisors: Dr. Dawei Yao, Riccardo Maria Fersini, Dr. Robert Andersson

(Traton AB)

Examiner: Full Professor, Louise Olsson

Abstract

The enforcement of the EURO VII legislation has introduced challenges for heavy-duty commercial vehicles. Severe conditions and extreme operational boundaries are considered when EURO VII legislation required the Engine Aftertreatment System (EATS) to oblige strict requirements. To concur with the cost and time-consuming constraints inherent in the traditional Synthetic Catalyst Activity Test (SCAT) bench, the concept of the virtual engineering development of a high-fidelity simulation model becomes indispensable. The study establishes a predictive and well-structured 1D kinetic model for ammonia adsorption on dual-site selective catalytic reduction (SCR) system by utilizing the engine development software AVL CRUISE M. To survive under the highly dynamic exhaust flows and non-linear kinetics, the model and kinetics were mathematically customized by User Coding Interface (UCI) together with step functions and sign formulas to maintain stability and stabilize the oscillations by coupling ordinary differential equations (ODE) in the background. Parameter optimization was taken by a three-step work with the sensitivity analysis based on a one-factor-at-a-time-approach with DoE-Taguchi L9 Array and proceeding the vector guess by introducing the results into Levenberg-Marquardt (LM) algorithm by MATLAB to avoid any potential local minima. The calibrated model was validated against conditions of various concentrations and gas hourly space velocities (GHSV). The model attempt to yield an outstanding mean absolute error (MAE) of 1.9% and root mean square error (RMSE) of 2.8% in the baseline condition but also performed an MAE of 4.5% and RMSE of 6.9 % in extreme conditions, demonstrating the fidelity for EURO VII aftertreatment system development.

Keywords: EURO VII, SCR kinetic Modelling, Taguchi Method, Levenberg-Marquardt Algorithm, 1D-CFD simulation

Table of Contents

List of Figures

List of Tables

List of Nomenclature

Acronyms and Abbreviations

1D-CFD - One-Dimensional Computational Fluid Dynamics

AVL - Anstalt für Verbrennungskraftmaschinen List (Simulation Platform Developer)

Cu-CHA - Copper-exchanged Chabazite (Zeolite Catalyst Structure)

DoE - Design of Experiments

EATS - Exhaust Aftertreatment System

LM - Levenberg-Marquardt (Optimization Algorithm)

MAE - Mean Absolute Error

ODE - Ordinary Differential Equation

OFAT - One-Factor-at-a-Time (Sensitivity Analysis Methodology)

RMSE - Root Mean Square Error

SCAT - Synthetic Catalyst Activity Test (Bench Experiment)

SCR - Selective Catalytic Reduction

SV - Space Velocity (1/h)

UCI - User Coding Interface (AVL Cruise M Platform Interface)

Chemical Nomenclature

NH_3 - Ammonia

NO_x - Nitrogen Oxides

N_2 - Nitrogen

H_2O - Water Vapor

Kinetic Parameters and Mathematical Symbols

A_ads1 - Pre-exponential factor for Site 1 adsorption (m3/kmol/s)

A_ads2 - Pre-exponential factor for Site 2 adsorption (m3/kmol/s)

A_des1 - Pre-exponential factor for Site 1 desorption (1/s)

A_des2 - Pre-exponential factor for Site 2 desorption (1/s)

Stor_Cu1 - NH3 storage capacity for strong adsorption Site 1 (mol/m3)

Stor_Cu2 - NH3 storage capacity for weak adsorption Site 2 (mol/m3)

E_a1 - Activation energy for Site 1 (J/mol)

E_a2 - Activation energy for Site 2 (J/mol)

R - Universal gas constant (8.314 J/(mol·K))

T - Localized absolute temperature (K)

θ - Surface coverage fraction of active sites

J - Jacobian Matrix (First-order partial derivatives matrix)

λ - Algorithmic critical damping factor for Levenberg-Marquardt updates

β - Parameter estimation vector (Magnitude for iterations)

1D Aftertreatment Simulation and Model Calibration for Euro VII Engines

Dennis Wang

Chalmers University of Technology, Gothenburg, Sweden

1. Introduction

1.1 Introduction to EURO VII and the aftertreatment systems

The EURO VII legislation has introduced unprecedented challenges for heavy duty commercial vehicles, the new legislation not only enforces tighter limits on NOx but also emphasizes the effect on extreme boundary conditions. For instance, cold start and real driving emissions are two main focuses. To satisfy the performance on these events, traditional and physical test benches no longer support the demand of such time-consuming and cost-prohibitive experiments, and this is when virtual engineering (e.g. 1D kinetic modelling) takes the lead in modern powertrain developments [1]. 1D modelling has the privilege on enabling engineers to ascertain the potential in the early development of rapid, iterate engines and exhaust systems on the EURO VII compliance [2]. Therefore, developers can accomplish a robust system to help improve the efficiency before any physical prototype takes the place by shifting the calibration and validation workload into virtual platforms. The exhaust aftertreatment system (EATS) are complex chemical reactors operated under dynamic and thermal exhaust flow conditions. To predict the tailpipe emissions accurately, high-fidelity mathematical models for each individual aftertreatment system components are required. Diesel Particular Filter (DPF), Catalysed Soot Filters (CSF) for trapping Particulate Matter (PM), Selective Catalytic Reduction (SCR) for NOx abatement and Ammonia Slip Catalyst (ASC), preventing the unreacted NH_3 to escape from the exhaust hereby acts as a series of components integrated into the EATS configuration [3]. Chemical reactions may differ in different counterparts of the aftertreatment system, the philosophy of modelling however can still be applied to the selective catalytic reduction (SCR) system, which serves as the main technology for NOx reduction in heavy-duty diesel commercial vehicles. Vehicle system simulations have proven the high efficiency for emission performance in different operational scenarios [4]. The EATS is required to maintain its exceptional NOx conversion efficiency across the fluctuating temperatures and mass flow rates under EURO VII. As the result, a precise 1D SCR model development is crucial for the engineering challenge with rigorous calibration and validation, and this forms the primary motivation for the research.

The macroscopic emission reduction in EATS requires a rigorous 1D kinetic model to accurately simulate and define the chemical kinetics in the catalyst. For modern SCR catalyst, the system utilizes metal-exchanged zeolites, such as Cu-CHA or iron-based zeolites in accordance with their thermal stability and high catalytic activity, with the

foundational structure dictating the reactivity [5]. The development of the digital twin model requires the first step on understanding the specific structure and reactivity relationships of the sites to define the equations and reactions of the model. Vanadium-based SCR (V-SCR) catalysts were widely used for commercial vehicles due to their cost performance and sulphur tolerances. Although V-SCR has the privilege over other type of catalysts mentioned above, the catalyst would exhibit the characterisation of thermal durability loss when conditions of extreme temperature occur. Historically, some global kinetic models assume a single type of site as a compromise for ammonia adsorption instead of two or more sites to minimize computational complexity. However, extreme conditions such as accuracy in heavy-duty EURO VII applications demand two or more active sites to be sufficient for modelling. Research on global kinetic modelling has demonstrated that copper-exchanged zeolites such as the Cu-SSZ-13 possess at least two dynamic sites for ammonia storage [6]. Therefore, adopting a two-site storage model for the research is quite imperative, with site 1 as the strong site (e.g. Cu^{2+}), responsible for high temperature desorption and site 2 the weak site (e.g. Brønsted acid sites), responsible for low temperature desorption. Although, two-site model introduces additional Arrhenius parameters and increases the complexity of calibration and validation indeed, predicting ammonia desorption dynamics across a broad working temperature for commercial vehicle accurately is undoubtedly necessary [7]. This ensures that the AVL Cruise M model reflects the physical limits of the catalyst. To implement the complex dual-site kinetic mechanisms within the simulation, conventional modelling will require look-up tables to approach the expected reaction rates [6]. However, operating conditions such as EURO VII could not be fulfilled by look-up tables, the model requires flexibility and resolution to accurately capture thermal and chemical shifts. To tackle the limitations, the research abandons the traditional table referencing method and utilizes mathematically defined step functions together with the user coding interface to approach dynamic and continuous control logic over kinetic parameters. This not only ensures the high fidelity of the simulation but also cultivates a robust design for the subsequent integration of the MATLAB algorithm, LSQCURVEFIT.

1.2 SCR kinetic Modelling

To establish a precise 1D model, the kinetic model must be grounded in the fundamental mechanisms of ammonia adsorption and desorption. It has been demonstrated that the catalyst's ammonia storage capacity must be defined strictly through the temperature programmed desorption (TPD) analysis before any macroscopic NOx reduction can be simulated [8, 9]. As NH_3 adsorption serves as the prerequisite step for subsequent catalytic reactions and simultaneously dictates the site availability, a group of accurate Arrhenius parameters for ammonia desorption

must be enhanced and thereby forms the foundation of steady-state kinetic modelling [8, 10, 11]. For heavy-duty vehicle applications, copper zeolites are selected over iron or manganese ones due to the superior low-temperature and robust performance [12, 13]. To capture the dynamics in the copper zeolites, a global kinetic model which accounts for at least two storage sites is imperative [10]. Although, real-world operations mostly run on transient-conditions, intrinsic parameters are isolated and initially validated under steady-state conditions. It is necessary to establish the steady-state model before introducing complex real-world variables, such as the dynamic SCR reactions for the presence of NO_2 [14].

Predicting the steady-state conversion is mathematically challenging, especially under various space velocity and inlet gas concentrations. Studies have shown that the measurement of the distribution of the inlet gas concentration varies significantly along the catalyst length [15]. Any minor inaccuracies of the parameters such as the pre-exponential factors or the desorption rate will lead to significant simulation errors for the validation and calibration of the model. Structured SCR models are provided by AVL to predict non-linear kinetic behaviours across different space velocities. However, models provided directly from the suppliers mostly function as black boxes and limits the ability to manipulate multi-site adsorption or detailed reaction mechanisms [7].

1.3 Catalyst aging and poisoning

Although, steady-state calibration for fresh catalyst cultivates the fundamental specs of the 1D-CFD simulation, comprehensive modelling for heavy-duty vehicles must also involve the further development to consider long-term exposure to harsh exhaust environments, as the exposure alters the active sites and kinetic parameters for copper zeolites. Operating under the EURO VII standard, catalyst systems are continuously exposed to severe chemical degradations, durability requirements once again point out the importance of considering aging environments. Phosphorus poisoning is considered as one of the primary chemical effects, studies have indicated that the phosphorus poisoning reactions interacting with Cu sites, impairs the performance of NH_3-SCRs [15, 16, 17, 18]. SO_2 poisoning from the exposure under SCR is another critical challenge. The formation of copper sulphates and ammonia sulphates blocks the pores and the active sites, forces the reaction to be paralysed [19,20]. Although, anodic sulphur poisoning can be concurred by the regeneration of catalyst through thermal management, the fluctuation of sites complicates the kinetic modelling [21, 22]. Exposure to high temperature and water vapor causes a permanent migration of active sites in the Cu-zeolite and thereby degrade the system's NO_X reduction performance [23, 24]. Although the research currently focuses on steady-state kinetics of fresh catalysts to eliminate the interferences and to cultivate the foundation of a

clear model, the acknowledgement of the aging mechanisms refreshes the value of the methodology. By getting rid of the SCR model provided by AVL, core kinetic equations and step functions can integrate the existing model with future development such as dynamic sites or various activation energies resulting from catalyst deactivation, the high-fidelity model could manipulate and expand itself into complex aging and poisoning simulation for future work.

1.4 Digital Twins and the automotive simulation

Digital twin serves as a virtual replacement of the physical system for mirroring the operational dynamics [25]. The integration of the technology has a huge economic impact on reducing development cycles and physical prototyping costs by optimizing the performance [26]. A highly predictive model is the core of any valuable and functional digital twin [27]. Therefore, to develop a model which survives under high-temperature processes on behalf of extreme thermal gradients and chemical environments in the Exhaust Aftertreatment Systems (EATS) becomes crucial [28]. The challenge sets as a foundation of 1D-CFD simulations to perceive fluid dynamics, kinetics and heat transfer accurately [24]. As the result, digital twins are therefore utilized for simulation in vehicle dynamics and powertrain interactions for developments [29]. The research employs AVL Cruise M, a widely recognized 1D simulation platform for advanced vehicle simulation [30]. AVL Cruise M offers the environment for implementing dynamic boundary conditions by customized coding tools engaged with python and visual C++ together with advanced use defined control logics. Conventionally, pre-compiled simulation model would suffer from loss of fidelity when extreme conditions or fluctuating boundary conditions occur, in contrast, a rigorous evaluation has demonstrated that a custom-coded model in AVL Cruise M could help prevent the loss and distortion [31]. Supported by strict Mean Absolute Error (MAE) and Root Mean Square Error (RMSE) evaluation, the mathematical framework establishes a precise and technical foundation for the virtual platform validation process.

Identification of the most sensitive variables among the parameters is fundamentally required prior to the final optimization of the model. Taguchi method is employed to achieve the goal by reducing the number of simulations required to practice and simultaneously maintaining a top-notch statistical confidence especially when complex non-linear interactions occur. The method conducts the orthogonal array to allow the systematic design for the experiments capture the possible combination and evaluate the primary effects of the various parameters including pre-exponential factor, desorption rate, activation energy and storage capacity within the two active sites [32, 33, 34]. Taguchi Method has been proven for its reliability and robustness for a wide

variety of fields ranging from performance tracking to quality control in diverse industries or even for the optimization of pulp production processes and electromagnetic applications for the design of antennas [35, 36, 37]. The proven methodology can be practiced to systematically isolate the tuning process among sensitive parameters.

1.5 The optimization methodology of kinetic parameters

Integration of algorithm is considered as an optimizing and widely recognized way to improve complex 1D-CFD kinetic modelling in modern engineering nowadays [38]. Due to the non-linear characteristics of Arrhenius chemical kinetics, manual calibration is indeed impossible to be implemented for the optimization, and therefore systematic computational methods are considered. Nevertheless, single-algorithm strategies would encounter limitations when sensitive computational fluid dynamics simulation (CFD) approaches. Gradient-based local optimization such as the Levenberg-Marquardt (LM) algorithm offers non-linear curve-fitting capabilities but depends on the initial quality of local minimum and guess. Nowadays, simulation optimization focuses on the necessity of combination within different strategies and has been demonstrated that coupling strategies with precise LM algorithm yields the success of avoiding local optimal traps [39]. Instead of relying on one single algorithm, the research adapts a combination of the Taguchi method to narrow down the boundaries, limitations and feed the guesses into MATLAB by conducting LM algorithm with the exact lsqcurvefit process. Two-step solver ensures the quality of the optimization remains on a high precision and fits the coded SCR model without distortions and loss of mathematical fidelity compared with traditional steady-state physical experiments.

To tackle the weakness of the model, the research chose to construct the SCR kinetic model by utilizing the user coding interface (UCI), mainly focusing on ammonia adsorption and storage as the critical process for the foundation of the model. From self-defined kinetic equations and step functions, flexibility is gained to capture the steady-state variations at extreme conditions such as a high space velocity or a low concentration. Evaluation of the error is taken by Mean Absolute Error (MAE) and Root Mean Square Error (RMSE) to quantify the deviation between the simulation and test data from SCAT experiments. Taguchi Method and LSQCURVEFIT algorithm are used to systematically calibrate the kinetic parameters.

2. Principle and Mechanisms of the validation and calibration process of SCR model

2.1 Establishment of the analysis model

The model is built via AVL Cruise M, R2024.R2 with Use Coding Interface (UCI) simulating the SCAT reactor. The model includes Mass Flow Boundary, Catalyst, System Boundary with Step Functions and Constants. The Mass Flow Boundary here defines the upstream gas that enters the system, with physical parameters such as the mass flow rate, temperature, pressure or gas species and concentrations. Catalyst hereby represents the physical Selective Catalytic Reduction (SCR), incorporated with channel geometry, washcoat properties, heat transfer dynamics and kinetic reactions. The downstream of the exhaust gas is represented by the system boundary, controlling the thermal conditions at the exit of the catalyst. Step functions and constant blocks act as the control and signal elements to impose the transient conditions during TPD or kinetic parameter validation procedures. Structure of the model is illustrated in Figure 1.

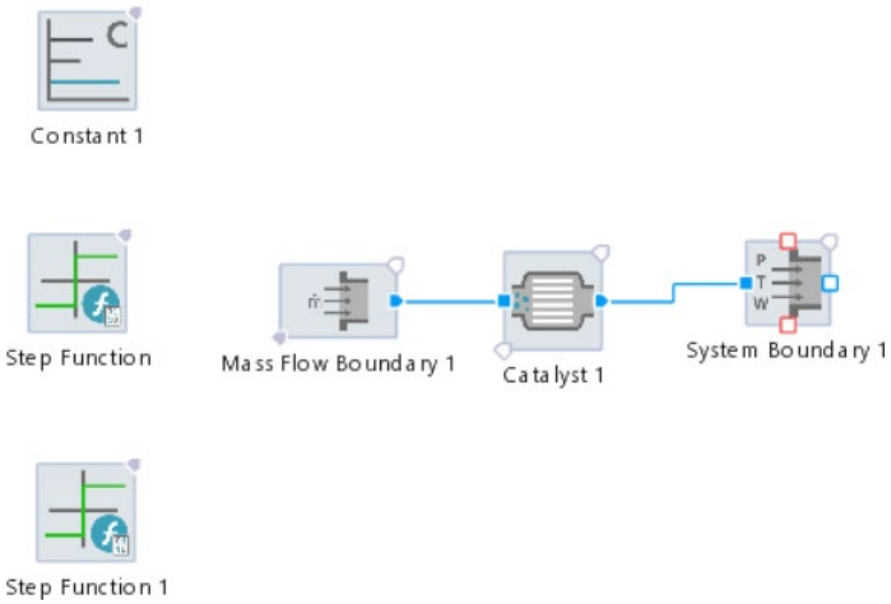

Figure 1 Overview of the selective catalyst reduction (SCR) model

Dimensions of the model

(1) Catalyst Material: Cordierite
(2) Catalyst Washcoat: Copper
(3) Volume: 0.01287 L
(4) Diameter: 25.3996 mm
(5) Cross sectional area: 506.69 mm^2
(6) Length: 25.4 mm
(7) Cell Density: 400 $1/in^2$
(8) Wall Thickness: 0.1016 mm

(9) Open Frontal Area: 0.7056
(10) Channel Structure: Square cell
(11) Geometrical surface area: 2897,64 1/m

2.2 Physical system of the study

The configuration of the engine aftertreatment system (EATS) is established by a one-dimensional (1D) flow model. The system evaluates the ammonia inlet/outlet and adsorption or storage capacity with different Temperature-Programmed-Desorption (TPD) programs, under various conditions such as the adsorption temperature, space velocity (GHSV) and concentration. Assuming uniform profiles and steady state conditions, the model optimizes the fidelity and efficiency of the simulation model. The system is simplified to consider ammonia (NH_3) as the direct injection to the inlet of the catalyst due to the complexity and loss of fidelity when urea-water solution appears to be involving further defects such as thermochemical decomposition or evaporation. As a result, this allows a dedicated evaluation of the washcoat reaction instead of confronting effects such as incomplete mixing or secondary urea deposit formation.

2.2.1 NH3 adsorption and TPD protocol setup

To systematically evaluate adsorption, storage capacity and the kinetics, the model was standardized to the test protocol from experiment conducted by Traton Germany. The following graph illustrates the TPD sequence under baseline condition of 1500PPM,80,000 1/h established in the SCAT experiment.

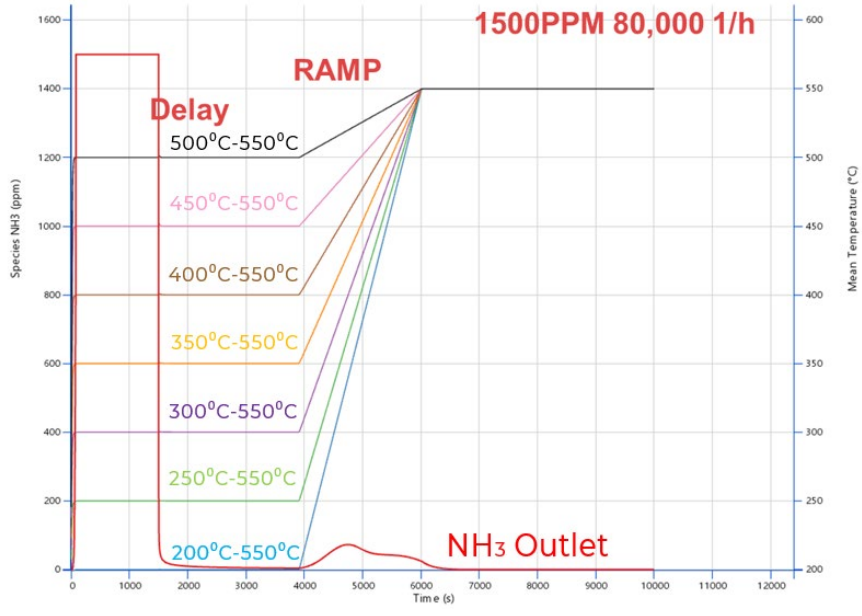

Figure 2 TPD sequence under baseline condition of 1500PPM,80,000 1/h

2.3 Model specification and assumptions

The solid substrate material of the catalyst is designated as Cordierite, providing a definitive geometric surface area, channel diameter and void fraction for monitoring mass transfer coefficients composed of a honeycomb structure. Conversely, the washcoat of the catalyst formed by copper zeolite which governs the active sites are decoupled via custom user coding interface (UCI) with the background logic consisted of Arrhenius equations. A setting of constants and step functions are served as control logic and limitations based on various TPD programs to avoid negative concentration integrations or ensuring the convergence of ordinary differential equations (ODEs) through different testing points.

2.3.1 The sensitivity test and parameter optimization workflow

The optimization process is executed across three sequential stages, with One-Factor-at-a-Time (OFAT), the sensitivity test was manually conducted to observe the potential impacts of the variables then input the identified sensitive parameters into the Taguchi orthogonal array. The structured approach would evaluate the interactions and establish the boundary limits for the third stage process. Algorithmic optimization would hereby be conducted, screening the dominant parameters and achieving high fidelity against the experimental data.

The optimization method is compulsory to manage the large variety of global parameters for Arrhenius kinetic equations. Replacing the black-box model with a user-defined model requires the estimation of numerous kinetic parameters, including adsorption/desorption pre-exponential factors, activation energies, and storage capacities, while conducting a simultaneous multi-variable test would lead to algorithmic divergence and local minima traps, localized sensitivity test can be utilized to isolate the dominant variables and set up a fundamental limit for sourcing and further optimization. One-Factor-at-a-Time (OFAT), the experimental method researchers normally use to observe the potential impacts of variables, is employed to support the background analysis of the sensitivity test. Secondary parameters are held as controlled variables with the target kinetic parameter as the independent variable to evaluate the trends, particularly the ammonia desorption peaks under the steady state TPD profile, sensitivity of each parameter within the cross-reference is therefore discovered. Highly sensitive variables which exhibit high gradients of reaction are then designated for Taguchi orthogonal array testing and algorithm filtering, but on the other hand the negligible trends are screened to be excluded from the following optimization process. The degree of freedom for the optimization process is hence

reduced and transformed into a high-fidelity calibration and validation procedure. The process of the sensitivity test is shown in the following figures. A_ ads1 represents the pre-exponential factor of site 1 adsorption, A_ ads2 represents the pre-exponential factor of site 2 Adsorption, A_ des1 represents the desorption rate of site 1, A_ des2 represents the desorption rate of site 2, Stor_Cu 1 represents the storage capacity of site 1 and Stor_Cu 2 represents the storage capacity of site 2.

A_ads 1	A_des 1	A_ads2	A_des 2	Stor_Cu 1	Stor_Cu 2
100000	1.00E+06	1000	1.00E+11	8.06	1.21E+01
1.00E+09	1.00E+06	1000	1.00E+11	8.06	1.21E+01
1.00E+12	1.00E+06	1000	1.00E+11	8.06	1.21E+01
100000	1.00E+08	1000	1.00E+11	8.06	1.21E+01
100000	1.00E+10	1000	1.00E+11	8.06	1.21E+01
100000	1.00E+12	1000	1.00E+11	8.06	1.21E+01
100000	1.00E+06	100000	1.00E+11	8.06	1.21E+01
100000	1.00E+06	10000000	1.00E+11	8.06	1.21E+01
100000	1.00E+06	1E+10	1.00E+11	8.06	1.21E+01
100000	1.00E+06	1000	1.00E+13	8.06	1.21E+01
100000	1.00E+06	1000	1.00E+15	8.06	1.21E+01
100000	1.00E+06	1000	1.00E+17	8.06	1.21E+01
100000	1.00E+06	1000	1.00E+11	80.6	1.21E+02
100000	1.00E+06	1000	1.00E+11	0.0806	1.21E-02
100000	1.00E+06	1000	1.00E+11	0.806	1.21E-01

Figure 3 The process of the sensitivity test, 1st attempt

100000	1.00E+03	1000	1.00E+11	0.24	3.60E-01
100000	1.00E+06	1.00E+07	1.00E+11	0.24	3.60E-01
100000	1.00E+06	1.00E+09	1.00E+11	0.24	3.60E-01
100000	1.00E+06	1E+12	1.00E+11	0.24	3.60E-01
100000	1.00E+06	1000	1.00E+10	0.24	3.60E-01
100000	1.00E+06	1000	1.00E+08	0.24	3.60E-01
100000	1.00E+06	1000	1.00E+06	0.24	3.60E-01
100000	1.00E+06	1000	1.00E+11	0.24	3.60E-01
100000	1.00E+06	1000	1.00E+11	0.12	1.80E-01
100000	1.00E+06	1000	1.00E+11	0.06	9.00E-02

Figure 4 The process of the sensitivity test, 2nd attempt

A_ads 1	A_des 1	A_ads2	A_des 2	Stor_Cu 1	Stor_Cu 2
100000	1.00E+06	1000	1.00E+11	8.06	1.21E+01
5.00E+04	1.00E+06	1000	1.00E+11	8.06	1.21E+01
1.00E+04	1.00E+06	1000	1.00E+11	8.06	1.21E+01
100000	1.00E+06	1000	1.00E+11	8.06	1.21E+01
100000	1.00E+07	1000	1.00E+11	8.06	1.21E+01
100000	1.00E+06	1E+13	1.00E+11	8.06	1.21E+01
100000	1.00E+06	1E+14	1.00E+11	8.06	1.21E+01
100000	1.00E+06	1E+15	1.00E+11	8.06	1.21E+01
100000	1.00E+06	1E+16	1.00E+11	8.06	1.21E+01
100000	1.00E+06	1000	1.00E+05	8.06	1.21E+01
100000	1.00E+06	1000	1.00E+04	8.06	1.21E+01
100000	1.00E+06	1000	1.00E+03	8.06	1.21E+01
100000	1.00E+06	1000	1.00E+11	0.024	1.21E-02
100000	1.00E+06	1000	1.00E+11	0.012	1.21E-03
100000	1.00E+06	1000	1.00E+11	0.006	1.21E-04

Figure 5 The process of the sensitivity test, 3rd attempt

A_ads 1	A_des 1	A_ads2	A_des 2	Stor_Cu 1	Stor_Cu 2
100000	1.00E+03	1000	1.00E+03	0.024	1.21E-02
100000	1.00E+02	1000	1.00E+03	0.024	1.21E-02
100000	1.00E+01	1000	1.00E+03	0.024	1.21E-02
100000	1.00E+03	1E+12	1.00E+03	0.024	1.21E-02
100000	1.00E+03	1E+13	1.00E+03	0.024	1.21E-02
100000	1.00E+03	1E+12	1.00E+03	0.024	1.21E-02
100000	1.00E+03	1E+12	1.00E+02	0.024	1.21E-02
100000	1.00E+03	1E+12	1.00E+01	0.024	1.21E-02
100000	1.00E+03	1E+12	1.00E+03	0.024	1.21E-02
100000	1.00E+03	1E+12	1.00E+03	0.012	1.21E-03
100000	1.00E+03	1E+12	1.00E+03	0.006	1.21E-04
100000	1.00E+03	1E+12	1.00E+03	80.6	1.21E+02
100000	1.00E+03	1E+12	1.00E+03	0.0806	1.21E-02
100000	1.00E+03	1E+12	1.00E+03	0.806	1.21E-01
100000	1.00E+03	1E+12	1.00E+03	0.06	9.00E-02

Figure 6 The process of the sensitivity test, 4th attempt

A_ads 1	A_des 1	A_ads2	A_des 2	Stor_Cu 1	Stor_Cu 2
100000	1.00E+06	1E+12	1.00E+04	0.024	1.21E-02
100000	1.00E+03	1E+12	1.00E+04	0.024	1.21E-02
100000	1.00E+06	1E+13	1.00E+04	0.024	1.21E-02
100000	1.00E+06	1E+12	1.00E+04	0.024	1.21E-02
100000	1.00E+06	1E+12	1.00E+04	0.024	1.21E-02
100000	1.00E+06	1E+12	1.00E+03	0.024	1.21E-02
100000	1.00E+03	1E+12	1.00E+03	0.024	1.21E-02
100000	1.00E+06	1E+13	1.00E+03	0.024	1.21E-02
100000	1.00E+06	1E+12	1.00E+03	0.024	1.21E-02
80000	1.00E+06	1E+12	1.00E+03	0.024	1.21E-02
100000	1.00E+06	1E+12	1.00E+02	0.024	1.21E-02
100000	1.00E+03	1E+12	1.00E+02	0.024	1.21E-02
100000	1.00E+06	1E+13	1.00E+02	0.024	1.21E-02
100000	1.00E+06	1E+12	1.00E+02	0.024	1.21E-02
1200000	1.00E+06	1E+12	1.00E+02	0.024	1.21E-02

Figure 7 The process of the sensitivity test, 5th attempt

A_ads 1	A_des 1	A_ads2	A_des 2	Stor_Cu 1	Stor_Cu 2
100000	5.00E+04	100000	5.00E+08	0.024	1.21E-02
100000	5.00E+04	100000	1.00E+08	0.024	1.21E-02
100000	5.00E+04	100000	1.00E+09	0.024	1.21E-02
100000	1.00E+04	100000	5.00E+08	0.024	1.21E-02
100000	1.00E+05	100000	5.00E+08	0.024	1.21E-02
10,000	5.00E+04	10,000	5.00E+08	0.024	1.21E-02
50,000	5.00E+04	50,000	5.00E+08	0.024	1.21E-02
200,000	5.00E+04	200,000	5.00E+08	0.024	1.21E-02
500,000	5.00E+04	500,000	5.00E+08	0.024	1.21E-02
100000	5.00E+03	100000	5.00E+09	0.024	1.21E-02
100000	5.00E+05	100000	5.00E+10	0.024	1.21E-02
5000	5.00E+04	5000	5.00E+08	0.024	1.21E-02
2000000	5.00E+04	2000000	5.00E+08	0.024	1.21E-02
100000	5.00E+04	100000	5.00E+08	0.048	1.20E-03
100000	5.00E+04	100000	5.00E+08	0.024	6.00E-03

Figure 8 The process of the sensitivity test, 6th attempt

2.3.2 Taguchi Method

Taguchi method is utilized for quality engineering to systematically conduct an effective parameter estimation. Unlike factorial designs that require an exponentially large matrix of simulation test cases, the Taguchi method employs orthogonal arrays to strategically sample the parameter space and is capable of evaluating parameters through a continuous evaluation of deviations and minimize the sensitivity of the model to noise, which serves as an ideal method for non-linear occasions. The fundamental theory of Taguchi method is monitored by the Taguchi Quadratic Quality Loss Function. A deviation of the simulated engine aftertreatment system (EATS) for the 1D-CFD chemical kinetic calibration contributes to a numerical loss in the Taguchi function, the relationship and comparison with the conventional method are shown in the following content.

$$L(y)=k(y-m)^2$$

L(y) represents the loss of quality, y represents the output value, m represents the target value and k represents the coefficient of the quality loss. Hereby, k, the quality loss coefficient stands as the engineering tolerance is interpreted as

$$k = \frac{\mathrm{A}}{\delta^2}$$

Where A indicates the prohibited lost cost when the system achieves the boundary, δ represents the distance between the target value and the Upper Specification Limit

(USL) or the Lower Specification Limit (LSL) therefore dictates the maximum possible allowance of the tolerance m± δ. Indeed, algorithm designed in the two-stage process for optimization is not eligible for filtering the runs of the simulation and would cause possible loss of fidelity. Therefore, difficulties for convergence may occur during algorithm filtering. In order to proceed a smooth process for the later on algorithm when computational economy is considered, the orthogonal array conducted by Taguchi method tackles the complex issue of practicing 4 independent kinetic variables with 3 discrete levels which equals to (3)^4=81 simulations to map the variables, the orthogonal array reduces the experiment attempt to merely 9 runs only. The method hereby eliminates the unpromising parameter regions and cultivates a tight boundary limit for the subsequent algorithmic optimization process.

The design of experiment (DoE) ensures equal distribution for the level of operation within every kinetic parameter and avoids the individual effects of the dominant variables. The optimization method is supported by the principle of combinatorial orthogonality. Orthogonality here according to the matrix algebra ensures the absolute geometric balance fund by the following two tenets.

Level	Factor A Stor Cu1		Factor A Stor Cu2		Factor C Ades1	Factor C Ades2
Level 1	175		255		4.00E+07	5.00E+09
Level 2	180		262		5.00E+07	8.00E+09
Level 3	185		270		3.00E+07	1.20E+10
	storcu1	storcu2	des1	des2	Error (mg/L)	
Run_1	175	255	4.00E+07	5.00E+09	54.26	
Run_2	175	262	5.00E+07	8.00E+09	90.8	
Run_3	175	270	6.00E+07	1.20E+10	126.33	
Run_4	180	255	5.00E+07	1.20E+10	127.47	
Run_5	180	262	6.00E+07	5.00E+09	38.53	
Run_6	180	270	4.00E+07	8.00E+09	81.82	
Run_7	185	255	6.00E+07	8.00E+09	72.14	
Run_8	185	262	4.00E+07	1.20E+10	115.45	
Run_9	185	270	5.00E+07	5.00E+09	39.77	

Table 1 DoE (Design of Experiment) conducted by Taguchi method

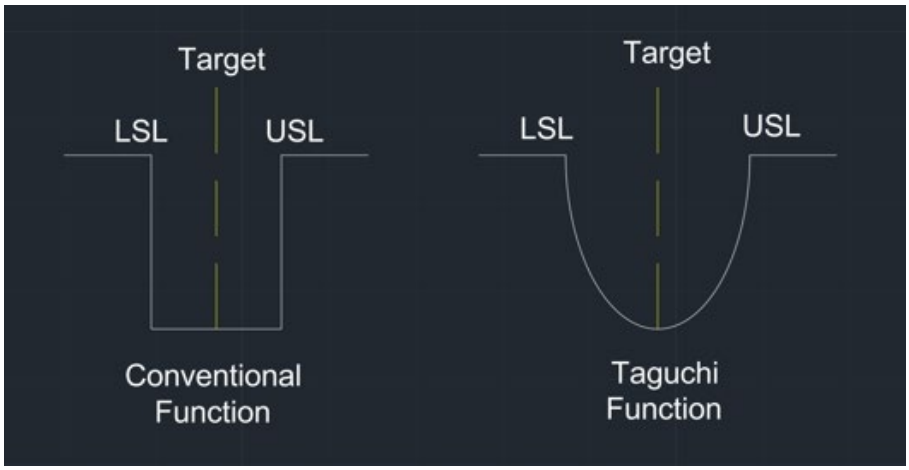

Figure 9 Comparison of the Taguchi function and the conventional function

2.3.3 Column-wise Uniformity and Pairwise Orthogonality

A level of balance appears as any level of the given column has the same probability of presence. For instance, a L9 array which involves 3 levels and 4 factors, the probability or the time when the certain level appears, remains equal for every individual (4 columns in this case). Moreover, when 2 of the factors are randomly compared, the possible combinations of the level also appear within equal amounts of chances. In short terms, the orthogonality ensures that every estimation of an individual factor would not be skewed by another.

According to the above mentioned, the orthogonality ensures that every estimation of an individual factor would not be skewed by another. This is achieved by the balance of levels, equal pairwise coverage and independence of the factors. Orthogonality has the privilege of accomplishing a drastic cost reduction, robustness and prioritizing the main effects. The orthogonal array is particularly advantageous due to its characteristic of ensuring the active sites are distributed equally through the entire tests. This consequently prevents the highly active variables from statistically dominating or concealing the secondary site kinetics. However, an isolation of interaction may occur due to the complexity of interactions, thereby algorithm is combined to revise the possible bias or for a fine-tune model fidelity.

2.3.4 Mathematical formulation of the SCR kinetics

The custom user coding interface is utilized to capture non-linear adsorption and desorption by formulating the chemical kinetics manually. The dual-site mechanism with site 1 representing the strong site1 and site 2 representing the weak site is defined

as the following reactions. R_f stands for the forward reaction and Rb stands for the backwards reaction.

$$R_{1f}: NH_3 + S_1 \longrightarrow NH_3 - S_1 \text{.....(1)}$$
$$R_{1b}: NH_3 - S_1 \longrightarrow NH_3 + S_1 \text{.....(2)}$$
$$R_{2f}: NH_3 + S_2 \longrightarrow NH_3 - S_2 \text{.....(3)}$$
$$R_{2b}: NH_3 - S_2 \longrightarrow NH_3 + S_2 \text{.....(4)}$$

Where S_1, S_2 represents the vacant active sites and $NH_3 - S_1$, $NH_3 - S_2$ represents the ammonia occupied sites.

Arrhenius kinetic rate constants

Fundamentally, the temperature-dependent rate constant determines the rate of each elementary reaction and is described by the Arrhenius equation. For instance, here the forward adsorption site 1 reaction has the rate constant k_{1f} expressed as

$$k_{1f} = A_{1f} \exp\left(-\frac{E1f}{RT}\right)$$

Where A1f represents the pre-exponential factor for R1f, E1f as the activation energy, R as the universal constant (8.314 J / (mol * K)) and T as the localised temperature by the absolute temperature unit. The above exponential structure could also be applied to evaluate kinetic rates on behalf of reaction k_{2f}.

In addition to the above, the actual reaction rate, taking once again the site 1 forward reaction as an example, with the local concentration and properties of the washcoat can be expressed as

$$Rate_{1f} = k_{1f} * ns_1 * \Theta s_1 * c\_NH_3$$

Where ns1 represents the total storage capacity or amount for site1 (mol/m³), ɵs1 as the vacant site coverage fraction of Site 1 and c_NH_3 as the localised ammonia concentration.

In contrast to adsorption, the backward reaction rate for desorption depends on the occupied site coverage

$$Rate_{1b} = k_{1b} * ns_1 * \Theta_{NH_3\text{-}S1}$$

and does not involve the gas-phase ammonia concentration c_NH_3.

Similarly, the above reaction rate structure could also be applied to evaluate kinetic rates for reactions R_{2f} and R_{2b}.

Ordinary Differential Equation (ODE) conservation, gradients and TPD Formulation

The coded reaction rates R1f, R1b, R2f and R2b are integrated into 1D equations to connect the microscopic chemical reactions rate with the macroscopic engine aftertreatment systems (EATS), this is theoretically supported by the following 1D transient species conservation equation.

$$\frac{dc\_NH3}{dt} + v_z \frac{dc\_NH3}{dz} = -[(Rate_{1f}\text{-}Rate_{1b}) + (Rate_{2f}\text{-}Rate_{2b})]$$

Where v_z represents the localised exhaust gas velocity in m/s along axis-z and c_NH_3 as the concentration gradient of ammonia. For temperature programmed desorption (TPD), the above differential equation results in a desorption peak rather than a continuous drop of ammonia concentration along the z direction across both two sites. The custom coded model integrates the ODE matrix across the finite grid and extracts high-fidelity conversion data. However, as TPD is inherently a transient process, the local temperature is defined as a linear function of time to capture the time-dependent behaviour.

$$T(t) = T_0 + ß\, t$$

Where T_0 is the initial adsorption temperature and ß as the heating rate, substituting the time-dependent profile T(t) into the Arrhenius equation yields a transient reaction as the following

$$k_{if}(t) = A_{if} \exp\left(-\frac{E_i f}{R\,(T0+ß\,t)}\right)$$
$$k_{ib}(t) = A_{ib} \exp\left(-\frac{E_i b}{R\,(T0+ß\,t)}\right)$$

k_b hereby grows exponentially as temperature increases over time and accelerates the thermal desorption, producing the ammonia desorption peaks observed through the TPD test.

2.3.5 Implementation of the control logic and the stabilizers within the user coding interface (UCI)

ODE nonetheless establishes the theoretical chemical background of the chemical kinetics integration to the model, however, to avoid possible divergence and to ensure

a robust design for the AVL Cruise M environment, control logic is implemented to the mass flow boundary of the simulated engine aftertreatment system (EATS).

2.3.6 Smooth boundary transition with step function

In typical TPD procedures, operational boundaries are normally controlled by look-up tables and standardized settings in the AVL Cruise M operational environment. Although the time-saving method may bring a reduction of time for an individual simulation to proceed, the data quality of the result may face difficulties maintaining a smooth and precise outcome or infinite gradient would temper the instability of the model. In other words, step function not only has the advantage of forcing the system to filter the numerical noise by interpolating a temporal delay (here as a delay time of δ =1 second) with a easily-accessible control logic but also an advanced platform for future development on more complex designs when various delay time is required or potential combination of algorithms or other optimization methods to prevent the loss of fidelity. The output of the step variable is defined by utilizing the following formulation.

$$\text{Out\_step(t)} = \begin{cases} v_0 & if \quad t < t_0 \\ v_0 + (v_1 - v_0) \times \frac{t - t_0}{\Delta t} & if \quad t_0 \le t \le t_0 + \Delta t \\ v_1 & if \quad t \ge t_0 + \Delta t \end{cases}$$

Non-physical suppression with conditional sign formulation

Negative values could appear in the numerical conversion under aggressive transient iterations for surface coverage fractions or localized concentration, causing irreversible or invalid algorithmic divergence and failure when conducted by exponential Arrhenius equations. For the prevention of failure, a set of sign limiters is directly implemented through the coded formulation, the logic is shown in the following content.

$$\text{Sign F} = \begin{cases} -1.0, & if \;\; C\_NH_3 < 0 \;^{(1-\theta<0)} < 0 \\ 1.0, & otherwise \end{cases}$$

Therefore, the intrinsic reaction rate is finally corrected into the following equation.

$$\text{Rate} = signF \times A_{ads} \exp\left(\frac{-E_{ads}}{RT}\right) \times C\_NH_3 \times Stor_{Cu} \times (1 - \theta)$$

This ensures that the reaction kinetics suppresses any potential mathematical oscillations and maintains a high-fidelity continuum for the 1D environment.

2.4 Algorithmic convergence strategy

Although, Taguchi method has the advantage to contribute to a robust design for the simulation model, the level-based principle, orthogonal array, limits the resolution of the calibration. To accomplish the convergence of a 1D-CFD model with experimentally determined targets, the non-linear algorithm, Levenberg-Marquardt, here in MATLAB as lsqcurvefit to tackle least-squares curve fitting problems, is served as the solver for the parameter estimation.

2.4.1 LSQCURVEFIT

The objective for the algorithm is to minimize the sum of squared residuals between the experimental target value and the simulated species across a certain amount of time or special nodes, it is expressed as the following formula.

$$S(ß) = \sum_{i=1}^{n}[y_i - f(x_i, ß)]^2 = r^T r$$

where ß serves as the kinetic parameters to be optimized such as the pre-exponential factor and desorption rate, y_i as the experimental target, $f(x_i, ß)$ as the output from the SCR simulation model and r as the residual vector.

2.4.2 Levenberg-Marquardt mechanism

The LM algorithm takes the responsibility of updating the parameter vector by evaluating the partial derivatives of the simulation output, forming the Jacobian Matrix **(J)**. Two optimization strategies are involved to govern the non-linear parameters from the ODEs and Arrhenius equations, the steepest descent method and the Gauss-Newton method, to determine the magnitude and direction. The formulation is shown in the following content.

$$[J^T WJ + \lambda\, \mathrm{diag}(J^T WJ)]\Delta ß = J^T W r$$

Where ß serves as the magnitude for the next iteration, J as the Jacobian matrix consist of the first-order partial derivatives ($\frac{\partial f}{\partial \beta}$), T as the transpose factor, W as the localized weighting matrix for highlighting the critical features and λ as the critical damping factor.

2.4.3 Algorithmic convergence strategy

The damping factor λ determines the critical modulation for the LM algorithm. λ would react according to the residual error, whether low or high, steepest descent method or Gauss-Newton method will be implemented. Gauss-Newton method takes the responsibility of maintaining localized convergence when the residuals decrease and the solver achieves the local minimum, oppositely, steepest descent method leads the role when the residuals are exceptionally high, then convergence is accomplished without overshooting. The custom 1D-CFD model achieves high fidelity by coupling the Taguchi method and the Levenberg-Marquardt (LM) algorithm, consequently allowing the real exhaust data to be consulted for Traton (VW Group)'s VTAB (Virtual Truck and Bus) platform.

3. Simulation Procedures

3.1 The numerical Discretization method

The grid configuration in the 1D-CFD environment is considered purely axial, in other words, the physical catalyst is discretized to a group of uniform volumes to simultaneously eliminate the errors and maintain the efficiency by Grid Independence Analysis, also known as the mesh convergence study. With negligible variations in the ammonia slip and conversion profiles, strict numerical stability is established to support the calibration matrices and all subsequent simulations.

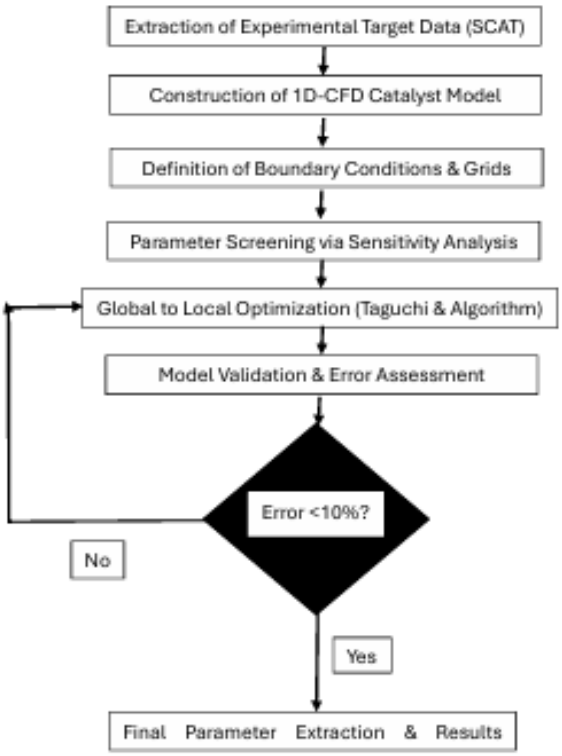

Figure 10 The workflow of the 1D-CFD modelling and optimization methodology

3.2 Experimental protocols and results

The experimental data from SCAT is conducted in Traton Germany. For Ammonia Temperature Programmed Desorption (TPD), the experiment is designed for the various programs consisting of different starting temperatures, concentration, space velocity (SV) and a stable temperature ramp, target temperature and delay time. Ammonia TPD consists of sequential stages of pretreatment, adsorption, purge and desorption. Pretreatment includes a preheated process under a carrier gas flow to clean the active sites and cultivate thermal stability. The reactor is later brought to the target adsorption temperature with a delay time until ammonia reaches its steady state breakthrough. Ammonia dosing is stopped but maintaining the carrier gas flow to purge weakly bounded ammonia from the pipeline. Desorption will then be practiced through the temperate ramping process and held for 15 minutes, generating desorption peaks measured by the analysers. The designed protocol is shown in the following table as an example of 1500PPM ammonia and a starting temperature of 200 ^{o}C.

Start Temperature (°C)	200	200	200	550
Target temperature (°C)	200	200	550	550
Temperature Ramp (K/min)			10	
Concentration H2O (ppm)	50000			
Concentration NH3 (ppm)	1500			
Aging [no(0), yes(1)]	0	0	0	0
MFC Adjustment [no(0), yes(1)]	0	0	0	0
Delay Time (min)	25	40		15

Table 2 Test protocol from Traton Germany from 200°C at 1500ppm

Start Temperature (ºC)	200	250	300	350	400	450	500
Target temperature (ºC)	550	550	550	550	550	550	550

Table 3 Test protocol for various temperature programs

Space Velocity (1/h)	500 ppm NH3	1000 ppm NH3	1500 ppm NH3
80,000	Tested	Tested	Tested
200,000	NA	Tested	NA
280,000	NA	Tested	NA

Table 4 Boundary conditions within SV and concentration for TPD test

3.3 Boundary conditions and integration interface

Strict boundary conditions are established in the catalyst model to systematically replicate the experimental environment within the 1D-CFD simulation model. The integration of the mass flow boundary and system boundary interface is employed to accomplish the goal. Ammonia (NH_3) is hereby injected into the system with various mass flow rate to match the space velocity (SV) which is eligible to mimic the exact SCAT testing environment with a constant pressure boundary condition of 1bar across the channels. The fundamental boundary conditions are shown in the following table.

Inlet Boundary	Mass Flow Rate	1.256 kg/h, 3.14 kg/h, 4.396kg/h
	Temperature Profile	Ramp (Input)
	Carrier Gas (Balance)	N_2
Outlet Boundary	Downstream Pressure	1.0 bar (Atmospheric)
	Thermal Boundary	Adiabatic / Mean heat source

Table 5 Fluid and thermodynamic boundary conditions of the 1D-CFD model

The relationship between the mass flow boundaries, catalyst (SCR) and system boundary is managed by the data bus connections by step function with automatic control and the user coding interface (UCI) dictating the chemical conditions in the underlying kinetics. Conditions such as the gas concentration or the solid-phase temperature are evaluated by each finite grid fed into Arrhenius equations each time step controlled by the step functions.

4. Results and Discussions

4.1 Establishment of the experimental baseline

The temperature programmed desorption (TPD) SCAT experiment was conducted in Traton Germany (MAN Truck & Bus). The SCAT experiment was conducted under various space velocities and concentration. The designed temperature programs mentioned above (As shown in table 2) are implemented for the SCAT test, from the initial temperature of 200 ^oC, 250^oC, 300^oC, 350^oC, 400^oC, 450^oC, 500^oC to a final temperature of 550^oC, with a stable ramp included in the program, recorded in the unit of mg per litre monolith.

4.2 Parameter screening and optimization via sensitivity analysis and the Taguchi method

Before implementing the Taguchi method for the screening and optimization process, a sensitivity test conducted to qualitatively evaluate the trend and influence on every individual factor for the simulated TPD test is practiced one at a time. Baseline parameter values were initialised from preliminary manual calibration and literature defaults. Several results have been revealed according to the stability of the desorption curve (As shown in Figure 3-8) to determine the stability boundaries. While all Arrhenius parameters (A_f, A_b, E_{af}, E_{ab}) govern kinetic behaviour, adsorption activation energy is in accordance to the literature given values, focusing on tuning pre-exponential factors. Storage capacity according to the theory dictates the limit of the maximum of what the catalyst can store and thereby determines the critical value

among the parameters for further optimization in algorithm development. The pre-exponential factor for desorption is strictly required to be adjusted as it controls the balance of the kinetics and prematurely influences the initial surface coverage. As defined, site 2, the weak adsorption site, which is responsible for the reaction under low temperatures, determines the starting coordinates of the desorption curve. Strong adsorption by site1 would severely inhibit the response of a distinct desorption peak. As the result, the imbalance between the desorption rates of the two sites would induce non-linear oscillations, a close match between the kinetic parameters among two sites is required for accomplishing an advanced performance on the calibration process.

According to the observation from the qualitative sensitivity test, the L9 orthogonal array practiced by the tachi method is executed to isolate the critical parameter for the ammonia desorption profile. The slope, or the gradient, is proportional to the magnitude of the influence. Therefore, a more intense gradient leads to a more decisive impact on the function, with the results shown in the following figure.

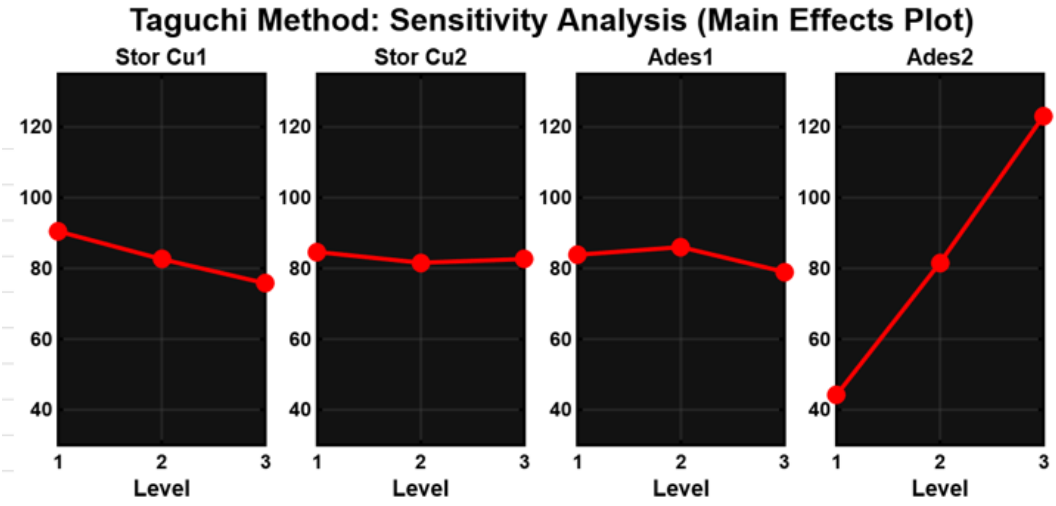

Figure 11 Results of critical parameter analysis from DoE, the Taguchi Method

Where the y-axis represents the Signal-to-Nosie Ratio (db). A_des2, the desorption rate of site 2, exhibits an exceptional gradient from level1 to level three. In other words, this confirms that the low temperature desorption rate turns out to be the most critical parameter in the system, with a decisive impact on the overall accuracy and controls the desorption peak fundamentally. In contrast, Stor_Cu1, the storage capacity of the strong site, site1, demonstrates a completely opposite trend. The negative slope indicates that although the parameter does not have strong effect on the kinetics but is still necessary to prevent failure for macrolevel baselines. Stor_Cu2, the storage

capacity of site 2, and A_des1, the desorption rate of site 1, remains horizontally across the levels, indicates that the model is robust to the variations of these parameters.

The optimization domain is narrowed down by DoE, the Taguchi method, and the desorption rate of site 2 should be prioritized in further optimization in the algorithm analysis due to its dominant effect on the simulation output. The convergence stability and the iteration efficiency can therefore be enhanced by the Levenberg-Marquardt (LSQCURVEFIT) algorithm, fixing the insensitive parameters and focusing on the highly sensitive variables. The parameter boundaries for Levenberg-Marquardt were mapped from the Taguchi orthogonal array. Highly sensitive parameters were centred around the Taguchi level 3 to allow fine gradient refinement. In contrast, less sensitive parameters were constrained around baseline levels to prevent algorithmic divergence.

4.3 Non-linear Algorithmic Tuning

Established in the former chapter, the Levenberg-Marquardt (LM) algorithm is practiced by the LSQCURVEFIT function in MATLAB. As the Taguchi method has identified the potential dominant parameters, the LM algorithm is executed to bridge the gap and achieve the non-linear convergence of the simulation. Combinations of the parameters are fed to the LM algorithm as the initial guess factor β. Insensitive factors such as the storage capacity of site 2 or the desorption rate for site 1 prevents the calculation of redundant partial derivatives from happening in the Jacobian matrix and accelerate the iterative speed of the ODE solver. The algorithm was thereby forced to stay in the highly accurate region of the levels from the design of experiments method.

4.4 Model validation and capability

The interest of the validation and calibration process is focused on the area under the adsorption/desorption curve from 3900s to 6500s among various temperature programs which is shown in the following figure.

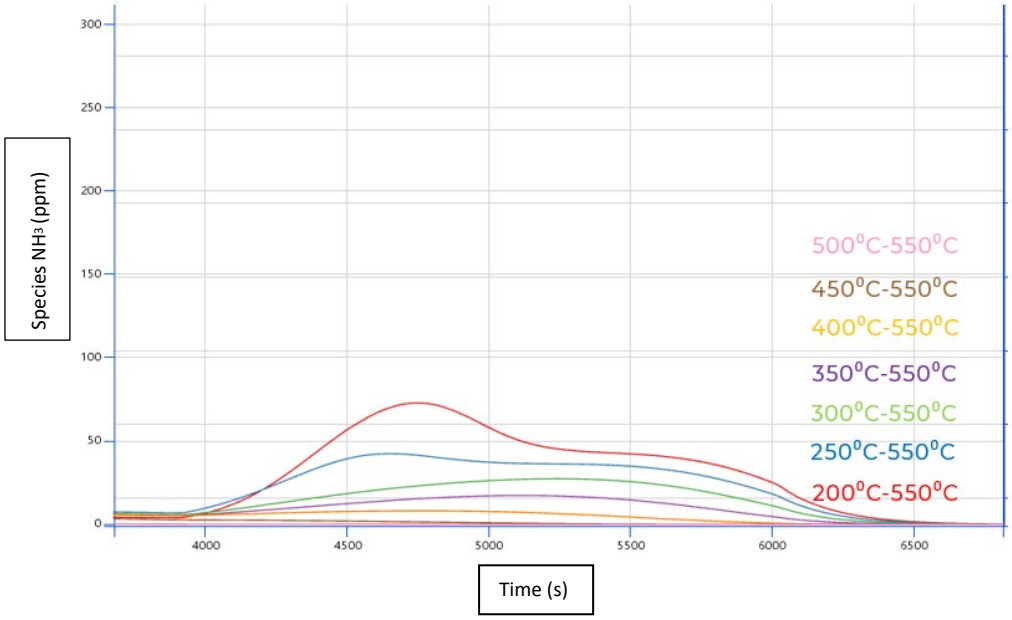

Figure 12 NH3 concentration and time comparison zoom-in at 3900s – 6500 s

The calibrated 1D-CFD model is utilized to initiate the validation against the SCAT experimental results. To ensure the fidelity of the model, both mean absolute error (MAE) and root mean square error are employed to evaluate the deviations, with MAE controlling the baseline of the overall evaluation and RMSE punishing the large localized deviations.

Mean absolute error (MAE)

$$\text{MAE} = \frac{1}{m}\sum_{i=1}^{m}\left|y_{test}^{(i)} - \hat{y}_{test}^{(i)}\right|$$

Root mean square error (RMSE)

$$\textbf{RMSE} = \sqrt{\frac{1}{m}\sum_{i=1}^{m}\left(y_{test}^{(i)} - \hat{y}_{test}^{(i)}\right)^2}$$

Where m represents the total number of data points, $y_{test}^{(i)}$ capture the measured ammonia concentration from the SCAT test and $\hat{y}_{test}^{(i)}$ as the predicted value from the 1D-CFD model.

The comparison of the 1D simulation model storage capacity and the SCAT experimental data points across the temperature spectrum are shown in the following figures.

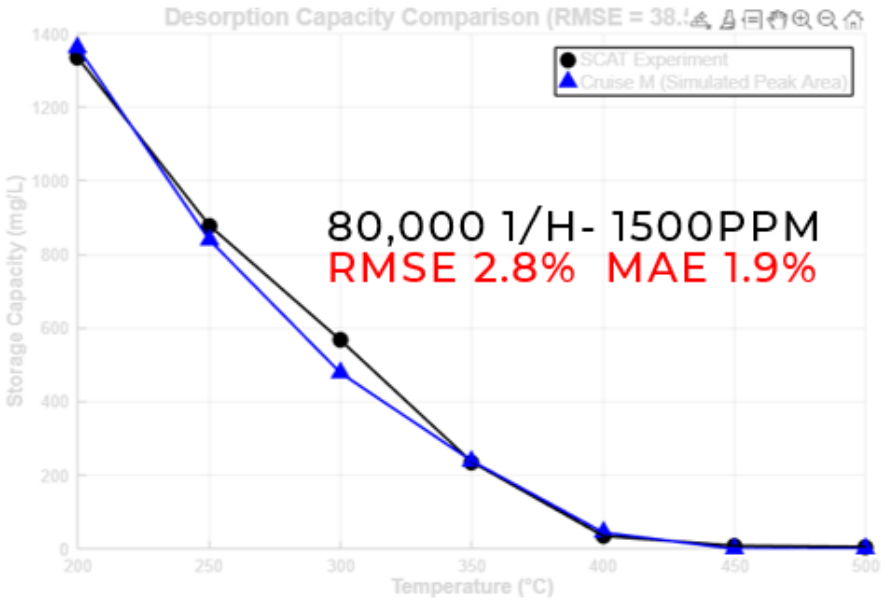

Figure 13 Error comparison, 80,000 1/h-1500ppm NH_3

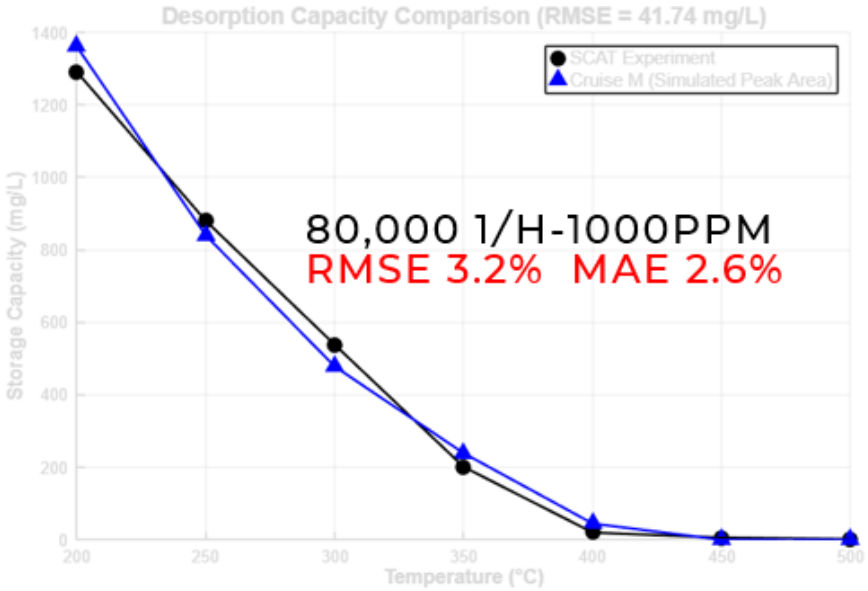

Figure 14 Error comparison, 80,000 1/h-1000ppm NH_3

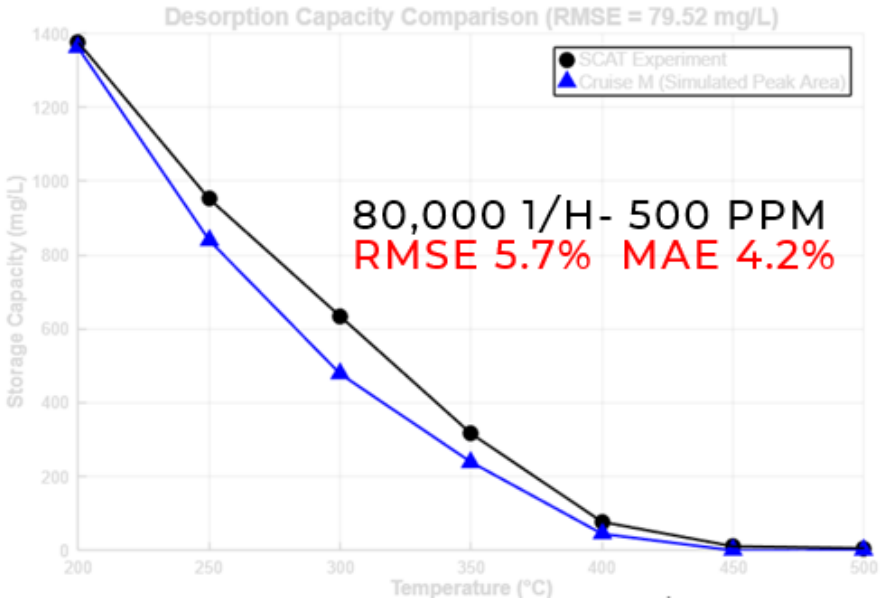

Figure 15 Error comparison, 80,000 1/h-500ppm NH_3

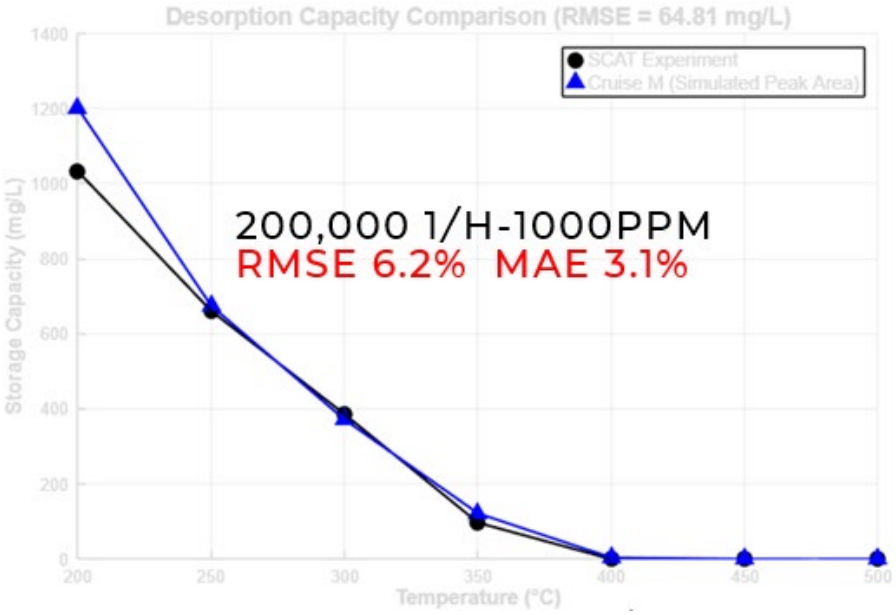

Figure 16 Error comparison, 200,000 1/h-1000ppm NH_3

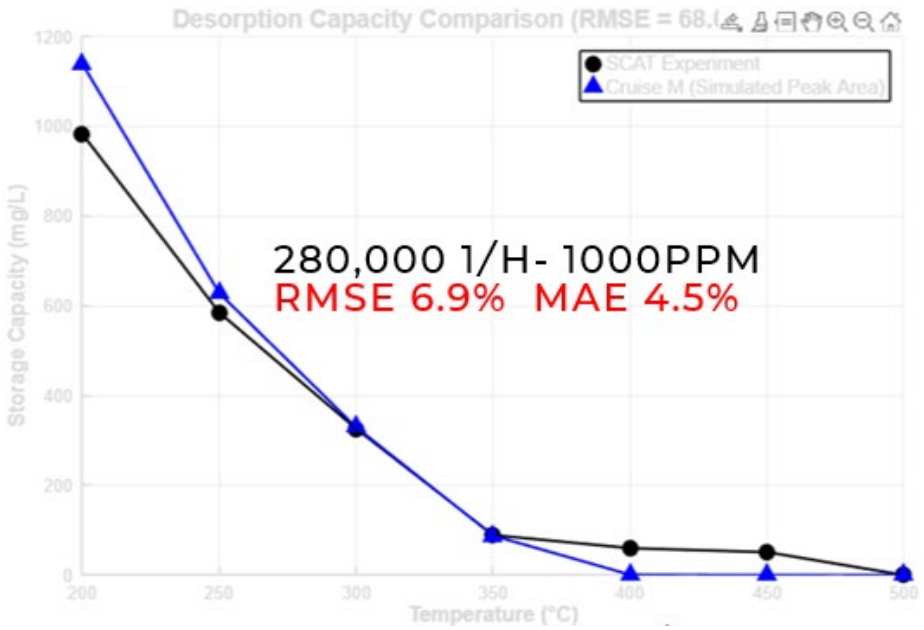

Figure 17 Error comparison, 280,000 1/h-1000ppm NH_3

The model accomplishes a highly robust accuracy. Under the baseline condition (80,000 1/h-1500ppm NH_3), which is the program used to calibrate the model, has an outstanding RMSE of just 2.8% and an MAE of only 1.9%. The model still survives and performs high quality when it comes to severe conditions such as the 280,000 1/h-1000ppm NH_3 program. These results demonstrate that the model maintains good predictive capability across the investigated operating conditions. In addition to the model's robust design, the capability to depict the TPD behaviour also comes to an important discussion to consider in the simulation. The results are shown in the following figures.

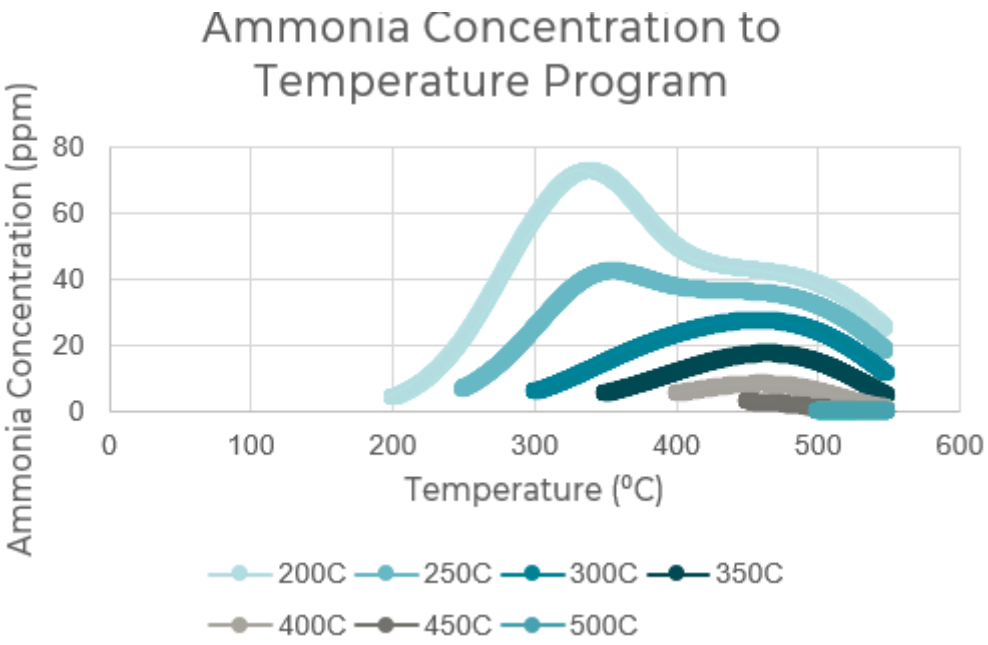

Figure 18 Ammonia Concentration to Temperature Program 80,000 1/h-1500PPM NH_3

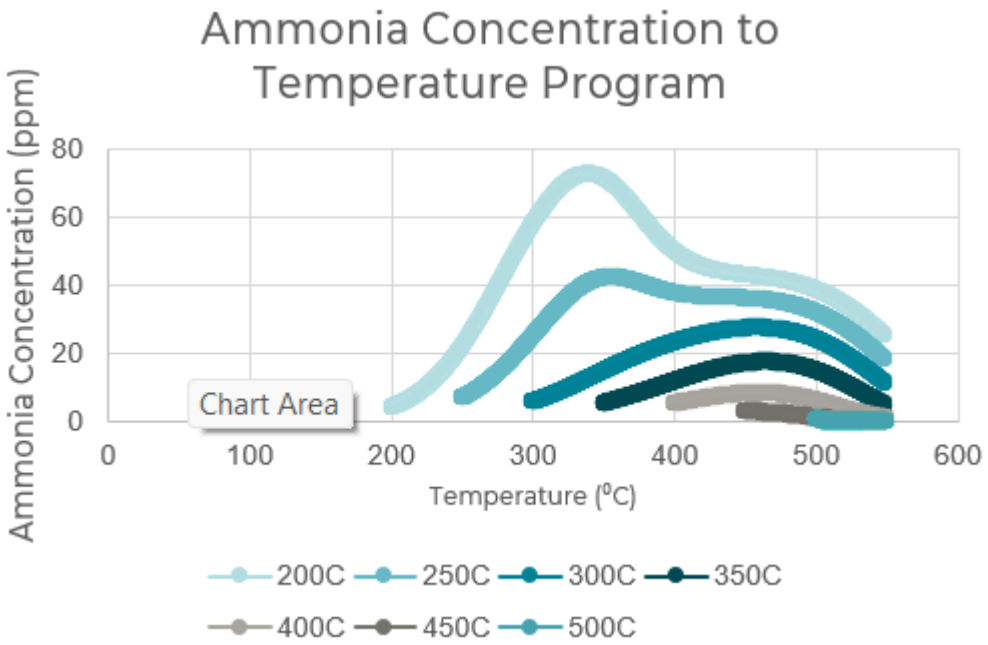

Figure 19 Ammonia Concentration to Temperature Program 80,000 1/h-1000PPM NH_3

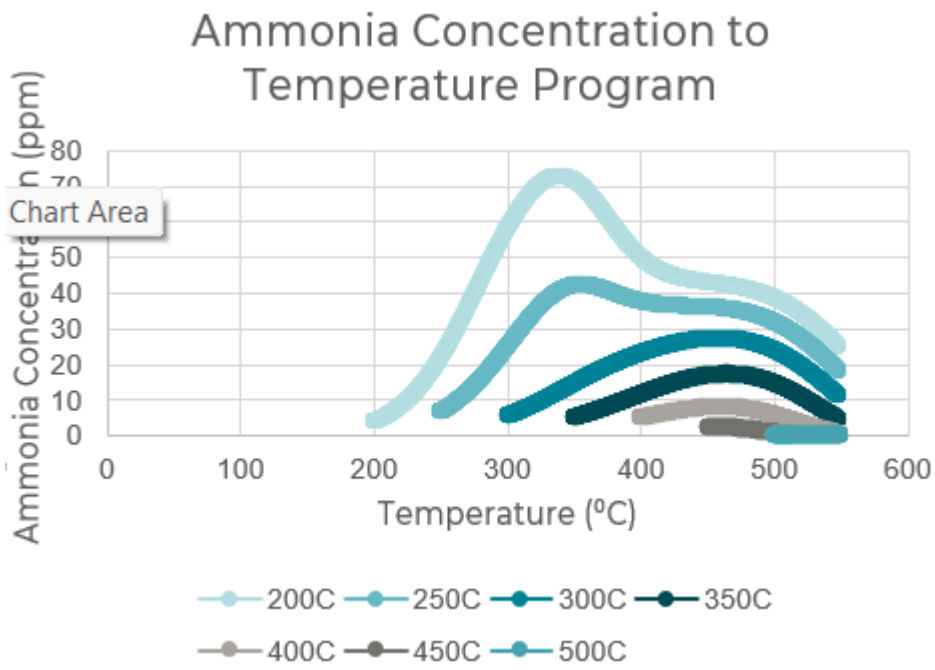

Figure 20 Ammonia Concentration to Temperature Program 80,000 1/h- 500 PPM NH_3

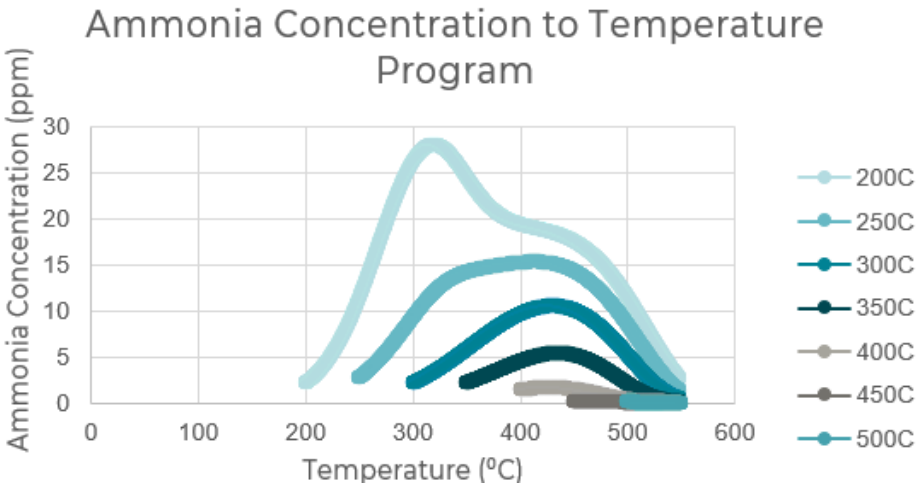

Figure 21 Ammonia Concentration to Temperature Program 200,000 1/h-1000PPM NH_3

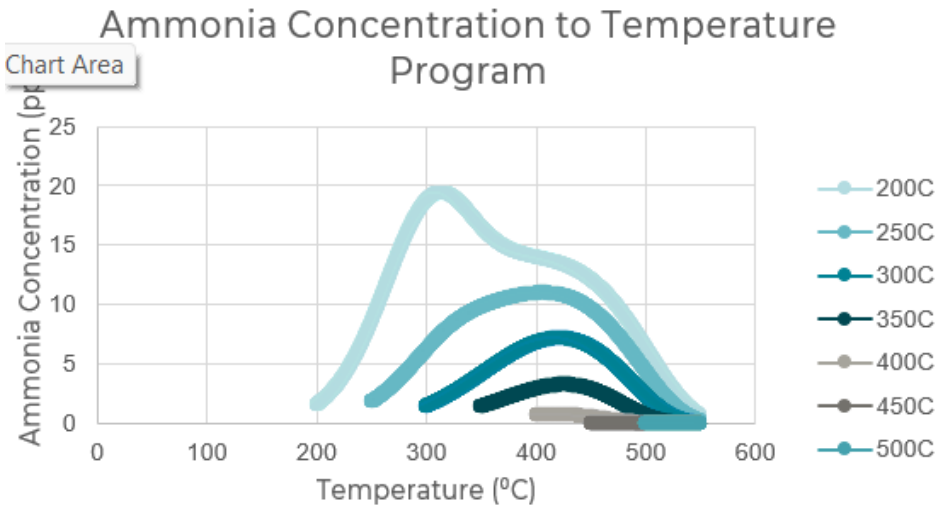

Figure 22 Ammonia Concentration to Temperature Program 280,000 1/h- 1000PPM NH_3

According to the above figures, the calibrated digital twin replicates the characteristic of a double peak in adsorption profiles. The model predicts the attenuation of the peak amplitudes when various temperature programs occur in the adsorption profiles, from the starting temperatures of 200 ^{o}C to 500^{o}C. Hence, the parameters including the pre-exponential factor for adsorption, desorption rate, storage capacity for both sites has now confirmed that the model perfectly mirrors the thermodynamic realities of the Cu-based catalyst.

5. Conclusions

The kinetics of Cu-based catalyst were successfully decoupled and calibrated by integrating the temperature programmed desorption (TPD) experiment together with multiple optimization methods such as the sensitivity test, DoE-Taguchi method as the screening method and algorithm-Levenberg-Marquardt (LM) as the numerical method. A 1D dual-site NH_3 adsorption/desorption model for a Cu-based SCR catalyst was established and calibrated. Unlike traditional and conventional transient methods, the experiment was designed for various starting points in the TPD protocols from 200^{o}C to 500^{o}C. This allowed the activation energies toward the weak site and strong site set as the foundation for further kinetics modelling. The L9 orthogonal array which was conducted by the Taguchi method has successfully screened the sensitivity of the individual parameters. This has proved that A_{des2}, the desorption rate of site 2 was the critical factor which governs the initiation of the desorption peak. Oppositely, the storage capacity of site 2 on the other hand exhibited its less-influenced sensitivity compared with other parameters, and this has undoubtedly narrowed down the computation process among optimizations.

By the cooperation of Taguchi array and non-linear LM algorithm, the model has confirmed its convergence. The strategy has avoided its potential of being trapped in local minima, resulting a highly robust vector of ß which mirrors the reality of the kinetic design. Final calibration was carried out with the baseline condition of 80,000 1/h-1500ppm NH_3 with a mean absolute error (MAE) of merely 1.9% and root mean square error (RMSE) of 2.8%. The model even accomplished an error of MAE 4.5% and RMSE of 6.9% only when performing in a severe condition such as the 280,000 1/h-1000ppm NH_3 environment. This confirms the model's capability to predict and easily surpassing conventional engineering acceptance, simultaneously demonstrating its potential for further integration into Euro VII aftertreatment system development.

While the 1D kinetic model elaborates its high fidelity on simulating high accurate SCAT environments, certain limitations remain. The current model addresses primarily on desorption and storage capacity kinetics. The expansion to complete a well-structured global kinetic model for copper-based catalyst including fast, slow and standard SCR as well as side reactions should be considered in future work. Furthermore, the development for future work could be implementing a data-driven predictive algorithm, capable of continuously optimizing kinetic biases. As a result, the algorithm could significantly reduce the development cost for keeping huge reliance on physical SCAT iterations by dynamically and precisely predicting the dosing quantities required under various transient conditions. However, the successful approaches for advanced algorithm and optimization method would require a massive and comprehensive experimental data from physical test benches (SCAT) to ensure a robust design for future model training and validation.

Acknowledgements

The author is grateful to Traton AB, Traton R&D Sweden for offering an inspiring environment for research and work and Traton R&D Germany for conducting the experiments.

Please accept my deepest gratitude for the instructions from my supervisors Dawei Yao, Riccardo Maria Fersini, Robert Andersson in Traton and Prof. Louise Olsson from Chalmers University of Technology with my managers Ragna Elger and Kim Petersson and my team and colleagues Christoph Sommer, Arnold Teglas, Anders Ersson and Pierre Sabucco. I would also like to extend my appreciation to Mayte Pach, Sara Lögdberg, Joakim Voltaire and Henrik Hittig for offering precious suggestions and a wonderful working environment.

My sincere appreciation goes to Prof. Sheng Guo, Prof. Emmy Cao and Dr. Wei Di from Chalmers University of Technology.

Last but not least, I would also like to thank you AVL for providing such an exceptional modelling software and Prof. Chen, Jyh-Chen from National Central University, Taiwan for inspiring my simulation knowledge since my undergraduate school and my family and friends who has been supporting me thousands of miles away. The thesis is dedicated to you.

References

[1] S. Wijeyakulasuriya, J. Kim, D. Probst, K. Srivastava, P. Yang, R. Scarcelli, P. K. Senecal, Enabling Powertrain Technologies for Euro 7/VII Vehicles with Computational Fluid Dynamics, Sciencedirect, 2022

[2] C. Limblici, Investigation of engine concepts with regard to their potential to meet the Euro 7 emission standard using 1D-CFD software, 2020

[3] T. Ovaska, M. Mikulski, K. Spoof-Tuomi, K. Lehtoranta, S. Niemi, P. Valkjärvi, T. Maunula, M. Mikulski, K. Lehtoranta, J. Alanen, M. Happonen, Effect of late diesel injection on close-coupled SCR + ASC during DPF regeneration period, ELSEVIER, Fuel, vol. 381, 2025

[4] C. Stuart Daw, Zhiming Gao, David E. Smith, Tim J. Laclair, Josh A. Pihl, K. Dean Edwards, Simulated Fuel Economy and Emissions Performance during City and Interstate Driving for a Heavy-Duty Hybrid Truck, SAE International, January 2013

[5] T. Jiang, Raul F. Lobo, On the Mechanism of Ammonia SCR over Cu- and Fe-Containing Zeolite Catalysts, Structure and Reactivity of Metals in Zeolite Materials, vol. 178, pp. 155-178, February 2018

[6] Y. Feng, Reaction kinetics of NH3-SCR over Cu-CHA from first principles, 2021

[7] Y. Feng, Ton V. W. Janssens, Peter N. R. Vennestrøm, J. Jansson, M. Skoglundh, H. Grönbeck, High-Temperature Reaction Mechanism of NH3-SCR over Cu-CHA:
One or Two Copper Ions?, THE JOURNAL OF PHYSICAL CHEMISTRY, vol. 128, pp. 6689-6701, 2024

[8] A. F, Suarez-Corredor, M. U. Bäbler, L. Olsson, M. Skoglundh, Björn Westerberg, Understanding the NH3 adsorption mechanism on a vanadium-based SCR catalyst: A data-driven modeling approach, ScienceDirect, 2022

[9] X. Song, G. Parker, J. Johnson, J. Naber, J. Pihl, A Modeling Study of SCR Reaction Kinetics from Reactor Experiments, SAE International, August, 2013

[10] Z. Gao, J. Pihl, T. LaClair, B. Fricke, Global kinetic modeling of NH3-SCR with two sites of NH3 storage on Cu-SSZ-13, ScienceDirect, 2021

[11] I. Khurana, J. D. Albarracin-Caballero, A. J. Shih, Identification and quantification of multinuclear Cu active sites derived from monomeric Cu moieties for dry NO oxidation over Cu-SSZ-13, ScienceDirect, 2022

[12] S. S. R. Putluru, L. Schill, A. D. Jensen, R. S. N. Fehrmann, Selective Catalytic Reduction of NOx with NH3 on Cu-, Fe-, and Mn-Zeolites Prepared by Impregnation: Comparison of Activity and Hydrothermal Stability, Hindawi Journal of Chemistry, Vol. 2018, pp. 1-11, August, 2018

[13] H. Söval, R. J. Blint, L. Olsson, Detailed kinetic modeling of NH3 SCR over Cu-ZSM-5, ScienceDirect, Applied Catalysis B: Environmental, 2009

[14] Y. Shan, G. He, J. Du, Y. Sun, Z. Liu, Y. Fu, F. Liu, X. Shi, Y. Yu, H. He, Strikingly distinctive NH3-SCR behavior over Cu-SSZ-13 in the presence of NO2, nature communications, August, 2022

[15] X. Auvraya, W. Partridge, J. Choi, Josh Pihl, F. Coehloa, A. Yezerets, K. Kamasamudramc, N. Currier, L. Olsson, Kinetic modeling of NH3-SCR over a supported Cu zeolite catalyst using axial species distribution measurements, ScienceDirect, Applied Catalysis B: Environmental, 2015

[16] S. Shwana, J. Janssonb, J. Korsgrenb, L. Olsson, M. Skoglundh, Kinetic modeling of H-BEA and Fe-BEA as NH3-SCR catalysts—Effect of hydrothermal treatment, ScienceDirect, Catalysis Today, vol. 197, pp. 24-37

[17] R. Daya, S. Y. Joshi, J. Luo, R. K. Dadi, N. W. Currier, A. Yezerets, On kinetic modeling of change in active sites upon hydrothermal aging of Cu-SSZ-13, ScienceDirect, Applied Catalysis B: Environmental, vol. 263, 2020

[18] A. Wang, M. E. Azzoni, J. Han, K. Xie, L. Olsson, Insight into the effect of phosphorus poisoning of Cu/zeolites with different framework towards NH_3-SCR, ScienceDirect, Chemical Engineering Journal, vol. 454, 2023

[19] J. Han, J. D. Bjerregaard, H. Grönbeck, D. Creaser, L. Olsson, Effect of SO_2 and SO_3 Exposure to Cu-CHA on Surface Nitrate and N2O Formation for NH_3-SCR, ACS Engineering, May 2024

[20] M. Attaran, B. G. Celik, Digital Twin: Benefits, use cases, challenges, and opportunities, ScienceDirect, Decision Analytics Journal, 2023

[21] K. Leistner, L. Olsson, Deactivation of Cu/SAPO-34 during low-temperature NH3-SCR, Applied Catalysis B: Environmental, ScienceDirect, vol. 165, pp. 192-199, 2015

[22] P. H. Ho, J. Shao, D. Yao, W. Di, D. Creaser, L. Olsson, ScienceDirect, Chemical Engineering Journal, vol. 418, 2023

[23] L. Wei, Y. Chen, S. Marino , Y. Gu, W. S. Epling, Kinetic modeling of NH3-selective catalytic reduction (SCR) over a mildly hydrothermally aged commercial Cu-SSZ-13 catalyst, ScienceDirect, Chemical Engineering Journal, vol. 467, 2023

[24] V. Mesilov, S. Dahlin, S. L. Bergman, S. Xi, J. Han, L. Olsson, L. J. Pettersson, S. L. Bernasek, Regeneration of sulfur-poisoned Cu-SSZ-13 catalysts: Copper speciation and catalytic performance evaluation, Applied Catalysis B: Environmental, vol. 299, 2021

[25] D. Thomas, Economics of Digital Twins, NIST Advanced Manufacturing Series NIST AMS 100-61, October, 2024

[26] H. Lam, E. Azar, D. Batur, S. Gao, W. Xie, S. R. Hunter, M. D. Rossetti, THE ECONOMIC IMPACT OF DIGITAL TWIN TECHNOLOGY ON MANUFACTURING SYSTEMS, Proceedings of the 2024 Winter Simulation Conference, 2024

[27] D. NEMES, T. PÁLFI, S. HAJDU, Vehicle Dynamic Simulation Possibilities Using AVL Cruise M, International Journal of Engineering and Management Sciences (IJEMS) Vol. 5, No. 2. 2020

[28] A. Kantaros, T. Ganetsos, E. Pallis, M. Papoutsidakis, From Mathematical Modeling and Simulation to Digital Twins: Bridging Theory and Digital Realities in Industry and Emerging Technologies, MDPI, Applied Sciences, 2025

[29] E. J. Lopez, N. M. Nigro, COUPLING STRATEGY BETWEEN 0D/1D AND MULTI-D CODES FOR THE SIMULATION OF COMPRESSIBLE FLOW PROBLEMS, May, 2011
[30] A. IORGA, ROAD VEHICLE SIMULATION USING AVL CRUISE, SCIENTIFIC BULLETIN, AUTOMOTIVE series, year XXI, no. 25, April, 2016
[31] S. HERMANSSON, S. VASANADU, Improvement of Shift Quality in Power-On Upshift using Motor Torque Control, 2016
[32] J. S. Ramberg, S. M. Sanchez, P. J. Sanchez, L. J. Hollick, DESIGNING SIMULATION EXPERIMENTS: TAGUCHI METHODS AND RESPONSE SURFACE METAMODELS, Proceedings of the 1991 Winter Simulation Conference, 1991
[33] F. Mistree, U. Lautenschlager, S. O. Erikstad, and J. K. Allen, Simulation Reduction Using the Taguchi Method, National Aeronautics and Space Administration, 1993
[34] J. Jiang, D. Legrand, R. Severn, R. Mikkulainen, A Comparison of the Taguchi Method and Evolutionary Optimization in Multivariate Testing, April, 2020
[35] C. L. Moller-Wong, The Taguchi Methods of quality control examined: With reference to Sundstrand-Sauer, 1988
[36] H. A. Y. Muhsen, TAGUCHI'S OPTIMIZATION METHOD AND ITS APPLICATION TO THE DESIGN OF ANTENNAS, August, 2009
[37] Hernadewita, Rochmad I., Hendra, Hermiyetti, Yuliani, E.N.S. An Analysis of Implementation of Taguchi Method to Improve Production of Pulp on Hydrapulper Milling, International Journal of Production Management and Engineering, 2019
[38] Y. Penga, C. Chenc, M. C. Fud, A review of simulation optimization with connection to artificial intelligence, ScienceDirect, Fundamental Research, 2026
[39] S. Amaran, N. V. Sahinidis, B. Sharda, S. J. Bury, Simulation optimization: a review of algorithms and applications, Ann Oper Res, vol. 240, pp. 351-380